

T_1 and T_2 spin relaxation time limitations of phosphorous donor electrons near crystalline silicon to silicon dioxide interface defects

S.-Y. Paik, S.-Y. Lee, W. J. Baker, D. R. McCamey,^{*} and C. Boehme[†]*Department of Physics and Astronomy, University of Utah, 115 South 1400 East, Salt Lake City, Utah 84112, USA*

(Received 4 May 2009; revised manuscript received 16 December 2009; published 25 February 2010)

A study of donor electron spins and spin-dependent electronic transitions involving phosphorous (^{31}P) atoms in proximity to the (111) oriented crystalline silicon (*c*-Si) to silicon dioxide (SiO_2) interface is presented for $[^{31}\text{P}] = 10^{15} \text{ cm}^{-3}$ and $[^{31}\text{P}] = 10^{16} \text{ cm}^{-3}$ at about liquid- ^4He temperatures ($T = 5 - 15 \text{ K}$). Using pulsed electrically detected magnetic resonance (pEDMR), spin-dependent transitions between the ^{31}P donor state and two distinguishable interface states are observed, namely, (i) P_b centers, which can be identified by their characteristic anisotropy, and (ii) a more isotropic center which is attributed to E' defects of the SiO_2 bulk close to the interface. Correlation measurements of the dynamics of spin-dependent recombination confirm that previously proposed transitions between ^{31}P and the interface defects take place. The influence of these electronic near-interface transitions on the ^{31}P donor spin-coherence time T_2 as well as the donor spin-lattice relaxation time T_1 is then investigated by comparison of spin Hahn-echo decay measurements obtained from conventional bulk sensitive pulsed electron paramagnetic resonance and surface sensitive pEDMR, as well as surface sensitive electrically detected inversion recovery experiments. The measurements reveal that the T_2 times of both interface states and ^{31}P donor electron spins in proximity to them are consistently shorter than the T_1 times, and both T_2 and T_1 times of the near-interface donors are reduced by several orders of magnitude from those in the bulk, at $T \leq 13 \text{ K}$. The T_2 times of the ^{31}P donor electrons are in agreement with the prediction by de Sousa that they are limited by interface-defect induced field noise.

DOI: [10.1103/PhysRevB.81.075214](https://doi.org/10.1103/PhysRevB.81.075214)

PACS number(s): 71.55.Cn, 72.25.Rb, 73.20.Hb, 76.30.Da

I. INTRODUCTION

Due to their technological importance, the properties of phosphorous (^{31}P) donors in crystalline silicon have been investigated extensively for more than half a century. During this time, magnetic resonance based methods have revealed many aspects of the microscopic nature of ^{31}P , as well as the electronic processes in which it is involved. Since the first mapping of a donor wave function using an electron-nuclear double-resonance technique,¹ a large and diverse amount of information regarding the electronic and quantum-mechanical properties of such systems has been reported.² This wealth of information has contributed to the technological exploitation of silicon to the extent that it has become the most widely utilized semiconductor in the global electronics industry. However, even with all the information regarding silicon available to us, there are still questions regarding the ability to exploit the quantum-mechanical nature (specifically spin) of dopants and charge carriers for technological applications such as spin transistors³ or quantum computers,⁴ the latter of which are proposed to utilize electron or nuclear spins of phosphorus donors in silicon as quantum bits. While there has been significant experimental effort toward the implementation of these and other concepts,⁵ challenges remain in a number of different areas, with the most pressing being the difficulty in detecting the spin of individual donors without reducing its quantum memory time (the coherence time T_2).⁶ Nevertheless, donors in silicon retain promise in this area due to their extremely long phase coherence times, with T_2 exceeding 60 ms for the electron spin⁷ and 1 s for the nuclear spin⁸ at liquid-He temperatures.

Many of the recent schemes for silicon based spin or quantum devices involve electronic processes occurring at or

near interfaces, particularly the *c*-Si/ SiO_2 interface. This presents advantages, since locating spins near interfaces allows them to be controlled with surface gates⁴ and to be detected with surface electronics.⁹⁻¹³ However, it may also lead to a decrease in spin coherence due to the spin-spin interactions with surface states,^{14,15} as well as to the loss of quantum information following spin-dependent recombination through surface states. Since it is not possible to obtain defect-free *c*-Si/ SiO_2 interfaces¹⁶ (we note that work is currently being undertaken to obtain defect-free interfaces using H termination but it is in the early stages^{17,18}) and since there are even proposals to use interface defects as probe spins to read out⁹ the spin of a single donor, the understanding of interface electron and spin transitions has become important.

In the following, pulsed electrically detected magnetic resonance (pEDMR) and pulsed electron-paramagnetic-resonance (pEPR) measurements performed on (111) surface oriented *c*-Si samples with $[\text{P}] = 10^{15} \text{ cm}^{-3}$ and $[\text{P}] = 10^{16} \text{ cm}^{-3}$ at temperatures between $T = 5$ and 15 K are presented. The data were collected in order to elucidate the nature of spin-dependent electronic interface transitions involving ^{31}P donor and interface states and to then determine how these processes influence the coherence time of the ^{31}P donor electron spins in proximity to these interface defects. The latter was accomplished by comparison of the interface sensitive pEDMR measurements to bulk sensitive pEPR measurements of ^{31}P donors. Our results are discussed with regard to their implications for the ability of spin-qubit readout using interface-defect probe spins while maintaining long coherence times. We emphasized that while the key questions motivating this study are centered about ^{31}P qubit coherence times, the study presented follows an extensive number of previous electron-paramagnetic-resonance (EPR),¹⁹⁻²⁵ elec-

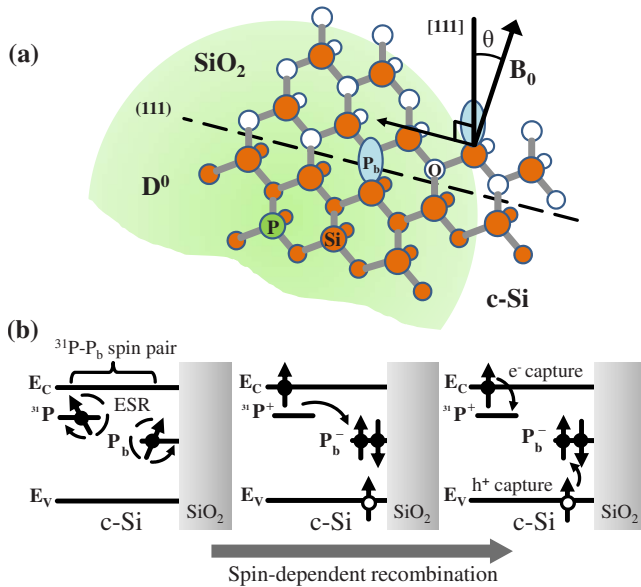


FIG. 1. (Color online) (a) Ball and stick illustration of the atom scale structure of the c -Si/SiO₂ interface. The ³¹P donor state (large green shaded circle) is significantly larger than the P_b center. Exchange coupling between the two states is possible when they are sufficiently close to each other. The orientation of the interface is defined by the angle θ between the externally applied B_0 magnetic field and the (111) crystal axis which is perpendicular to the crystal surface. (b) Band sketch illustrating the spin-dependent ³¹P/P_b recombination transition. For details see the text.

trically detected magnetic-resonance (EDMR),^{10,25–28} and pEDMR (Refs. 29–31) studies carried out on various c -Si/SiO₂ interface defects as well as electronic trapping and recombination processes of interfaces with different surface orientations and ³¹P doping concentrations. Most of these studies aimed to enhance the understanding of electronic processes relevant for materials systems used in conventional c -Si based microelectronics and photovoltaic devices. Thus, the study presented here may also be of relevance for conventional silicon technologies.

II. EXPERIMENTS

Following the recent demonstration of electrical detection of ³¹P spin states¹⁰ we anticipate, for the pEDMR measurements presented here, the presence of spin-dependent recombination between ³¹P donor states and energetically lower c -Si/SiO₂ interface states, as illustrated for the example of the P_b interface state in Fig. 1. Figure 1(a) displays a geometrical stick and ball sketch of the c -Si/SiO₂ interface where some of the silicon (111) surface atoms possess unsaturated bonds (called dangling bonds). These dangling bonds are all oriented along the (111) axis²⁵ and are highly localized states with much p content and only small s content.^{32,33} Silicon dangling bonds oriented along the (111) direction (also called P_b centers) are highly anisotropic and, since they are paramagnetic when uncharged,^{19,34} can be identified using EPR by their well-known Landé (g) factor anisotropy,²⁵ revealed by measurement of EPR spectra as a function of the

angle θ between the B_0 field and the (111) direction (see sketch). In contrast to the P_b state, the shallow ³¹P donor state [illustrated by the large shaded circle in Fig. 1(a)] is a significantly less localized state having an s -like envelope function with a localization length of ≈ 3 nm, strongly modulated by the periodic crystalline structure of its host environment.^{35,36} Since the ³¹P donor state encompasses thousands of silicon sites, an exchange interaction between near-surface ³¹P donors and P_b centers can occur, allowing the transition of the donor electron into the energetically lower interface state. This transition is sketched for an interface band diagram in Fig. 1(b). The illustration shows that (i) both the ³¹P donor state as well as the P_b state become charged (positively and negatively, respectively) through the transition. (ii) Because of the Pauli principle, and spin conservation due to the weak spin-orbital coupling of silicon, the transition is spin dependent. Hence, the transition provides a spin-to-charge conversion mechanism and as a result, since the charge of the ³¹P⁺/P_b⁻ can be detected through the measurement of recombination currents, ³¹P/P_b pairs have been proposed as electric readout mechanism for ³¹P qubits.^{9,10}

Experimentally, time domain measurements of spin-dependent c -Si/SiO₂ interface recombination were conducted in order to verify that the qualitative behavior of interface currents after EPR excitation of the ³¹P or the P_b states is similar to higher doped c -Si samples with (100) orientation. In order to also verify electrically detect spin-Rabi oscillation (as expected from previous studies^{6,10}), transient-nutation-like measurements of the integrated current transients as a function of the excitation lengths were carried out. Following these preparatory measurements, four experiments were performed to address the following questions:

(i) Is the EDMR signal that has previously been observed¹⁰ at magnetic fields between the two hyperfine split lines of the ³¹P for measurements conducted at X -band excitations (approximately 10 GHz) truly due to P_b states? If so, are P_b states the only interface states involved in spin-dependent transitions as illustrated in Fig. 1(b) or are there other states at or near the interface, or even in the bulk, which could contribute to the observed signals? To address this question, a systematic study of the EDMR spectrum (the magnetic field dependence) as a function of the interface orientation angle θ was made in order to observe all g factors involved in spin-dependent recombination and to detect possible anisotropies of these centers.

(ii) Are the observed spin-dependent processes truly due to pairs of ³¹P and interface states as depicted in Fig. 1(b) or are the signals corresponding to different g factors due to independent processes? In order to address this question, a series of different spin-dependent current transients was recorded under various temperatures, light intensities, surface orientations, sample voltages and offset currents, as well as excitation powers and lengths. For all applied conditions, the current transients (a) were recorded after resonant excitation of the two ³¹P lines and (b) the interface states and the correlation between the dynamics of ³¹P and interface states were compared.

(iii) As our understanding about the nature of the interface defects and the transitions between interface defects and the

^{31}P donor electrons was established, the main question of this study was addressed: are the coherence times of ^{31}P donors near-interface defects compromised? For this, a series of coherence time (T_2) measurements was carried out on ^{31}P donors in proximity to interface states and with the same samples, under the same conditions (in fact, during the same experimental runs), the coherence time of bulk ^{31}P was measured for comparison. For the interface T_2 measurements, modified Hahn echoes, detected with pEDMR, were used in a similar way as recent studies of ^{31}P doped *c*-Si samples with (100) orientation⁶ and spin-dependent ^{31}P bulk processes at very high magnetic fields.³⁷ For the bulk T_2 measurements, conventional ESR detected Hahn-echo experiments were carried out. This comparative study of T_2 times was made as a function of the temperature for $5 \leq T \leq 13$ K.

(iv) Finally, in order to obtain information on whether the spin-coherence times T_2 of near-interface-defect ^{31}P are determined by the electronic transitions between ^{31}P and interface states or by the interface-defect induced spin-spin relaxation processes as suggested by de Sousa,¹⁵ a comparison of electrically detected T_2 times and T_1 times was made for a temperature of $T=5$ K. In order to measure T_1 , electrically detected inversion recovery measurements were performed.

III. EXPERIMENTAL DETAILS

For the experiments presented in the following, we used 300- μm -thick (111) surface oriented silicon since P_b centers for this surface are all identically oriented. This is in contrast to the (100) surface previously used for similar experiments^{6,10} as the (100) surface allows silicon dangling bonds (here they are called P_{b0} states) to exist in two orientations at the same time, which makes their individual spectroscopic identification with EPR as well as their differentiation from other possible interface defects very difficult. The experiments were conducted with dopant concentrations of $[\text{P}]=10^{15}$ and 10^{16} cm^{-3} , less than the 10^{17} cm^{-3} of previous EDMR studies.^{6,10} The lower concentrations ensured that interactions between neighboring ^{31}P atoms which are known to exist³⁸ at $[\text{P}]=10^{17}$ cm^{-3} can be neglected.

In order to enable the electrical detection of spin coherence, the *c*-Si samples required contact structures which would not strongly distort the homogeneity of the spin-resonant microwave fields B_1 . This problem was solved using a method similar to previous pEDMR studies at X band^{10,39}—we designed long matchlike sample substrates on which electrical sample contacts outside the microwave field are connected to the sample via ~ 50 -mm-long thin-film Al wires whose thickness of 100 nm is below the penetration depth of the applied microwave radiation. The contact structures were fabricated using a photolithographical lift-off process that was carried out after the Al film was evaporated on the H-terminated silicon (111) surface of the *c*-Si samples that had been prepared by a wet treatment with hydrofluoric acid. In order to maximize the density of interface states, a native oxide was grown on the (111) surface after the contact deposition by exposure of the sample to ambient air.

All EDMR and EPR experiments were carried out at X band using a cylindrical dielectric low- Q pulse resonator

which was part of a Bruker Elexsys E580 EPR spectrometer. The sample temperatures were obtained with a ^4He flow cryostat, the excess charge carriers were induced through a spectral cold light source (IR and UV filtered spectral light) with an incandescent light source (Schott KL 2500 LCD) with lamp temperature of about 3000 K producing an integrated spectral intensity of approximately 5 W cm^{-2} at the sample surface. The EDMR experiments were conducted by establishing a constant offset photocurrent using a constant current source with a time constant in excess of the experimental shot repetition time. Current transients were digitized and recorded, following current amplification by a Stanford Research SR570.

The raw data recorded for the presented measurements were a combination of spin-dependent currents and microwave induced artifact currents. The latter can be recorded separately by measurement of the current response at off-spin-resonant B_0 fields. Magnetoresistance effects on the microwave induced currents can be linearly extrapolated for *c*-Si at the given magnetic fields. The microwave current transients obtained from this procedure were subtracted from the raw data in order to reveal the current transients solely caused by spin-dependent transitions.

IV. MEASUREMENT RESULTS

A. Identification of spin-dependent transitions

1. Experimental data

In order to confirm the results of Stegner *et al.*¹⁰ for a *c*-Si:P/SiO₂ interface with smaller ^{31}P concentration and a (111) surface orientation of the silicon sample, transient measurements of photocurrent changes ΔI were recorded under various illumination conditions and temperatures. Figure 2 displays a data set of $\Delta I(B_0, t)$ recorded as a function of the magnetic field B_0 and the time t after a 96-ns-long microwave pulse with a frequency of $f=9.749$ GHz and a power of $P \approx 8$ W for $T=5$ K and a constant photocurrent of $I=270$ μA . The sample orientation was $\theta=0$. The data set clearly confirms the expected EPR induced currents with three local response maxima at $B_0=346.37$, 347.9, and 350.55 mT. The two outer peaks which are separated by a magnetic field of ≈ 4.2 mT are the two hyperfine lines of the ^{31}P donor electron while the peak close to the low-field (LF) ^{31}P line has been attributed to interface-defect states.¹⁰

2. Discussion

The transient behavior at the magnetic fields with EPR responses confirms the measurements by Stegner *et al.*¹⁰ It consists of a brief photocurrent quenching after the pulse, attributed to an enhancement of the interface recombination, followed by a longer-lived current enhancement. This enhancement arises because the density of singlet states returns to its steady state faster than the triplet states, causing a net quenching of the recombination rate.^{10,40} Note that variations of the temperature, the sample voltage, and therefore the photocurrent as well as the illumination conditions change the quantitative dynamics of the observed transients—they do not, however, change the qualitative quenching and en-

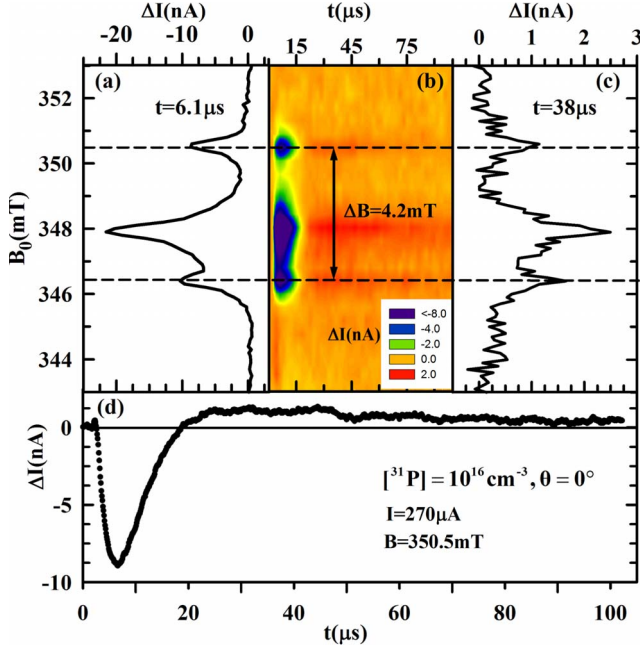


FIG. 2. (Color online) Plots of the microwave pulse (at $t=0$) induced change ΔI of an interface photocurrent along a c -Si(111):P/SiO₂ interface as a function of time t and the applied magnetic field B_0 . (a) and (c) Plots of ΔI as functions of B_0 for the times $t=6.1$ and $38 \mu\text{s}$, respectively, for which a quenching and an enhancement of the current changes reach their extrema. (b) Color contour plot of the entire data set $\Delta I(t, B_0)$ containing the data of the plots in (a), (c), and (d). (d) Plot of ΔI as a function of the time t for a magnetic field $B_0=350.5 \text{ mT}$ which was on resonance with the high-field ^{31}P EPR line.

enhancement behavior displayed by the data set in Fig. 2, which were also observed in previously reported measurements¹⁰ on c -Si(100):P/SiO₂ with $[\text{P}]=10^{17} \text{ cm}^{-3}$.

Both the quenching and the enhancement shown in Fig. 2(d) are well fit with simple exponential decay functions, in agreement with the observation of Stegner *et al.*¹⁰ This is somewhat counterintuitive since the random spatial distribution of the paramagnetic states involved in these transitions (see the discussion in Sec. IV B) suggests that the distances between pairs of paramagnetic states between which spin-dependent transitions occur are widely distributed. This distance distribution of states also implies a distribution of transition times,⁴¹ which suggests that the observed current transient quenching and enhancement should each be distributions of exponential functions for which fits with single exponentials would be poor. In contrast, the observed quenching and enhancement transients are well fit by two single exponentials, which suggests that only a narrow range of transition times exists and, therefore, only pairs with a narrow range of intrapair distances contribute to the observed signals. We attribute the existence of a “main-pair distance” which dominates the observed signals to two factors: first, pEDMR signals vanish for pairs with very large distances (larger than the localization length of the two paramagnetic states⁴¹) as the probability for recombination is greatly diminished and, second, for very short distances, where the exchange between the two states exceeds the Larmor fre-

quency difference within the pair,⁴² the signal vanishes as the resonantly induced change in spin-pair states between singlet and triplet configurations becomes increasingly forbidden.⁴² Thus, there will always be a finite main-pair distance where spin-resonance induced rate changes become maximal and pairs around this distance will dominate the observed spin-dependent currents.

B. Identification of interface defects

1. Experimental data

The data presented in Fig. 2 confirm that spin-dependent interface recombination processes can be observed with pEDMR at the c -Si(111):P/SiO₂ interface which are qualitatively similar to those seen previously at the c -Si(100):P/SiO₂ interface with higher ^{31}P concentration. It is therefore possible to systematically study the nature and the origin of the resonances found. Figure 3(a) displays the magnetic field dependence of the pulse induced photocurrent change $\Delta I(B_0)$ at times t after the pulse when the photocurrent changes were maximal (in the following referred to as the pEDMR spectra) for five different surface orientation angles ($0^\circ \leq \theta \leq 90^\circ$) and two ^{31}P concentrations. Note that while $\Delta I < 0$, the data have positive signs as each displayed spectrum was normalized to its respective extremum. The normalization was made for better comparison of the data sets since the signals obtained from samples with $[\text{P}] = 10^{16} \text{ cm}^{-3}$ were significantly stronger compared to signals from samples with $[\text{P}] = 10^{15} \text{ cm}^{-3}$ (note the higher relative noise in the latter spectra).

The fits of the pEDMR spectra required at least four different Gaussian peaks. A comparison with the ^{31}P EPR and EDMR spectra found in the literature^{10,43} allows immediate identification of the peaks at the highest and lowest magnetic fields as the well-known hyperfine split ^{31}P donor electron resonances. There are at least two additional resonance signals present. As these additional peaks are very close to each other and to the low-field ^{31}P hyperfine resonance, significant ambiguity for the 12 fit parameters (peak centers, width, and magnitude for all four lines) is present. This was overcome by a stepwise fit of the spectra: we first determine the ^{31}P spectrum and subsequently fit the two remaining non-phosphorous lines (eliminating six fit parameters). The separation of the low-field ^{31}P hyperfine line from the strongly overlapping nonphosphorous lines was achieved by first fitting the high-field (HF) ^{31}P hyperfine peak, which has little or no overlap with the other resonances, with a single Gaussian line. From the result of this fit, we can determine both the position (assuming a hyperfine splitting of $A=4.18 \text{ mT}$ as verified by bulk EPR measurements) and shape (assuming only negligible nuclear polarization, which is justified for the given sample temperatures and magnetic fields B_0) of the low-field ^{31}P hyperfine peak. The residue following these fits is then able to be fit with two Gaussian resonances. The full fit, as well as the four constituent peaks, is shown for all spectra in Fig. 3.

Figure 3(b) shows the g factors of the non- ^{31}P lines as a function of the angle θ , obtained from the fit. It also displays

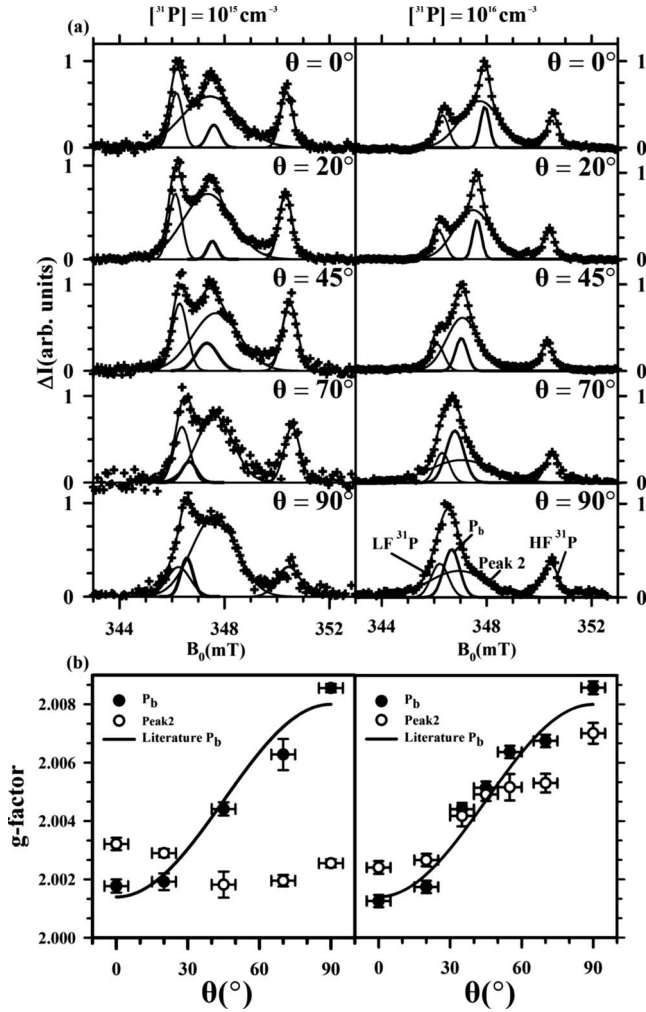


FIG. 3. (a) Plots of ΔI as a function of B_0 at arbitrary times t after a microwave pulse with arbitrary length τ , frequency $f \approx 9.5$ GHz, and a power $P=8$ W and under otherwise identical conditions as for the data in Fig. 2. The data were collected for five sample orientations θ and two ^{31}P concentrations. The displayed plots are normalized to the maximum of ΔI . The solid lines represent fits of the data consisting of four Gaussian peaks: two related to the ^{31}P hyperfine line and two peaks related to interface defects. The plot for $[^{31}\text{P}]=10^{16} \text{ cm}^{-3}$ and $\theta=90^\circ$ has the peak assignments to the LF and HF ^{31}P resonances, the P_b peak as well as peak 2. (b) Plots of the fit results of the g factors for the two interface-defect lines as a function of θ for the two ^{31}P concentrations. The solid lines indicate the literature values for the P_b center.

a solid line which represents literature values for EPR (Ref. 25) and EDMR (Refs. 29 and 31) detected P_b centers.

2. Discussion

The anisotropy and absolute value of the g factor of one of the two peaks are in excellent agreement with the P_b literature values for both ^{31}P concentrations. Based on this agreement, this peak can be assigned to spin-dependent transitions (recombination) which involve P_b centers. Note that previous pEDMR measurements on $c\text{-Si}(111)/\text{SiO}_2$ interfaces with no ^{31}P doping have shown P_b signals.^{29,31} Since

there are no ^{31}P pEDMR lines in intrinsic $c\text{-Si}$, it is clear that spin-dependent P_b interface recombination does not necessarily require the presence of ^{31}P atoms. Thus, the P_b involvement revealed by the data in Fig. 3 may either involve ^{31}P as illustrated in Fig. 1(b) or be due to an independent interface recombination process.

In contrast to the P_b resonance line, the assignment of the second non- ^{31}P peak [referred to as peak 2; see peak assignment in Fig. 3(a)] is less straightforward. The fit results for $[P]=10^{15} \text{ cm}^{-3}$ suggest that peak 2 is isotropic, or only weakly anisotropic, whereas the data for $[P]=10^{16} \text{ cm}^{-3}$ are consistent with an anisotropic peak. There are two explanations for this difference between the two sets of spectra: (i) that the nature of peak 2 is different at higher ^{31}P concentrations, suggesting that the observed processes may be different and (ii) that the fit error of the center g factor of peak 2 becomes increasingly inaccurate for larger values of θ . The latter may be due to the width of peak 2 and the relative weakness of the peak 2 intensity in comparison to the signal strengths of the P_b and ^{31}P EDMR signals at higher dopant concentrations, becoming increasingly problematic for the fit accuracy at large θ as three resonances (low-field ^{31}P , P_b , and peak 2) have larger overlap at higher angles. Note that the error ranges given in the plots in Fig. 3(b) are based on the uncertainty estimates of the fit routines. As additional uncertainties with regard to fit induced systematic errors are likely to exist, the true standard deviation for g factors of peak 2 may be significantly larger. Thus, it is not clear whether the different results for g factors of peak 2 obtained for different ^{31}P concentrations are real or fit artifacts and therefore an unambiguous statement about the anisotropy of peak 2 is not possible.

Previous pEDMR spectra on intrinsic $c\text{-Si}$ have shown a second isotropic recombination signal with $g \approx 2.0023(6)$.³¹ This is in good agreement with peak 2 observed on $c\text{-Si}$ samples with $[P]=10^{15} \text{ cm}^{-3}$. As with the previous study on intrinsic silicon, it is difficult to unambiguously assign peak 2 to a particular interface-defect type. Due to its strong inhomogeneity (the large linewidth) and its overall magnitude in comparison to the other pEDMR lines, it is possible that peak 2 is due to one or more randomly oriented anisotropic centers whose powder spectra would cause a macroscopically isotropic wide resonance line. The g factor and the linewidth are close (yet not equal) to the g factor and the linewidth of silicon dangling bonds in amorphous SiO_2 (so-called E' centers²⁵). Thus, it is possible that the observed pEDMR data are due to transitions involving E' centers in proximity to the $c\text{-Si}/\text{P}/\text{SiO}_2$ interface. Note that there are several distinct E' centers which differ by the backbonds of the Si atom on which the center is located (one or more oxygen atoms and hydrogen atoms) or their relaxation state (the unrelaxed E' center has been called E'_δ).²⁵ Charge-carrier trapping and recombination may work similarly for both the P_b centers with well-defined orientation as well as the randomly oriented E' . Due to the localization length of the ^{31}P donor electron state,³⁵ it is also conceivable that transitions between the shallow donor states and the deep interface states are possible. Hence, peak 2 is assigned in the following to an E' center with unspecified nature except for its proximity to the $c\text{-Si}/\text{P}/\text{SiO}_2$ interface.

C. Identification of ^{31}P to interface-defect transitions

1. Experimental data

The plots in Fig. 3 demonstrate the involvement of at least three qualitatively different paramagnetic electron states (^{31}P , P_b , and E') in spin-dependent charge-carrier recombination transitions. This observation, however, does not prove that the observed recombination transitions take place *between* these different states. While the spin dependency of transitions through localized states requires the existence of pairs of paramagnetic states,⁴⁴ there are examples of spin-dependent transitions which produce only a single resonance line in EDMR experiments^{28,39} when transitions occur between identical centers or when the paramagnetic pairs are strongly coupled. Therefore, the detection of multiple EDMR lines (as in Figs. 2 and 3) leaves the exact nature of these transitions elusive.

One approach to an understanding of whether the observed g factors belong to the same or different transitions is to analyze the dynamics of the spin-dependent processes associated with these different resonances: spin-selection rules usually discriminate permutation symmetries of spin $s = \frac{1}{2}$ pairs,^{40,42} which means that it is the mutual orientation of the two spins, not the individual spin state of one of the two pair partners, which determines the transition rate. Therefore, the transient behavior of spin-dependent transition rates exhibits an identical behavior after a spin-resonant manipulation of either one of the two pair partners. If two EDMR detected resonances exhibit a different transient behavior after the same pulsed excitation, the spin-dependent transitions corresponding to these resonances must be different as well. However, even if the transient behavior is identical, the two resonances may belong to identical transitions. While the different dynamics of spin-dependent transition rates for different g factors is a proof that they belong to different processes, identical transition rates only indicate that the two resonances may be due to the same process, as they may also be due to different processes which coincidentally have the same transient behavior. Therefore, the observation of identical transients requires further testing of the correlation of the observed dynamical behavior under varying experimental conditions.

Figure 2(b) demonstrates that the fast relaxing current quenching and the slowly relaxing current enhancing behavior discussed above occur similarly for both the ^{31}P hyperfine resonances and the resonances associated with interface states. The dynamics (which means the decay times of the different exponential functions), but not necessarily the absolute magnitude of current transients from different centers involved in the same electronic process, are identical. Thus, a comparison of different transients yields information about the paramagnetic centers between which transitions take place. We compare the “zero-crossing time,” τ_0 , defined as the time after the pulsed excitation of a spin-resonance induced current transient when the quenching and enhancement are identical. The comparison as shown in Fig. 2(b) clearly reveals identical $\tau_0 \approx 18 \mu\text{s}$ with an error of $\approx 1 \mu\text{s}$. This suggests that the processes connected to these resonances are due to transitions involving both the ^{31}P donor

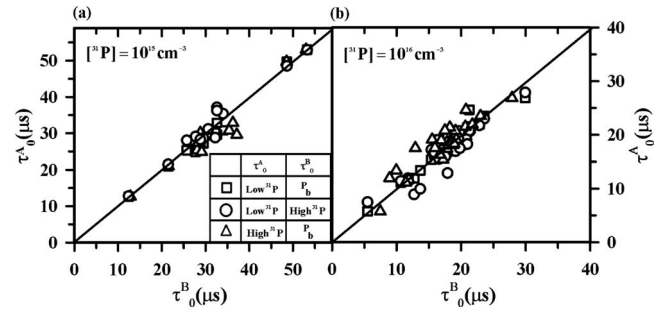


FIG. 4. Plots of the zero-crossing times τ_0 of magnetic resonantly induced photocurrent transients of the ^{31}P low- or high-field resonance (τ_0^A) versus the zero-crossing times of magnetic resonantly induced current transients of the P_b/E' center resonances (τ_0^B) measured for a variety of different samples and sample conditions (temperature, offset current, and illumination). The solid line is a linear function through the origin with a slope of 1. The two plots made for the two concentrations show a strong correlation of the zero-crossing times of all three resonances.

states as well as the P_b interface state or the E' near-interface state in the way depicted in the sketch in Fig. 1(b).

In order to test whether τ_0 for the interface defects and the ^{31}P remained identical when the dynamics of the spin-dependent current signal is changed, the experiment presented in Fig. 2(b) was repeated under various combinations of temperatures (5, 8, 10, 13, and 15 K), sample currents [10–300 μA (and therefore different electric fields)], and sample surface orientations for the two different ^{31}P doping concentrations mentioned above. Due to the variation in charge-carrier concentration as well as Fermi and quasi-Fermi energies caused by changing these experimental parameters, the dynamics of the observed spin-dependent recombination transitions, and therefore the dynamics of the observed current signals, changed significantly between measurements. For all data sets, τ_0 was determined for transients recorded at magnetic fields corresponding to the two ^{31}P hyperfine resonances as well as at the maximum of the overlapping interface-defect signals. The results of this procedure are displayed in Fig. 4 in two correlation graphs, for samples with the two different donor concentrations. Each graph displays a plot of τ_0^A versus τ_0^B with A and B corresponding to the ^{31}P low-field and the ^{31}P high-field resonances, respectively (represented by the circles); the ^{31}P low-field and the interface state resonances, respectively (represented by the squares); and the ^{31}P high-field and the interface state resonances, respectively (represented by the triangles).

2. Discussion

The data in Fig. 4 reveal three observations:

(i) As anticipated, the variation of experimental parameters clearly varies the dynamics of the observed signals.

(ii) While similar combinations of experimental parameters were used for the two concentrations, the times τ_0 of the samples with $[\text{P}] = 10^{15} \text{ cm}^{-3}$ are generally slower than the τ_0 obtained for $[\text{P}] = 10^{16} \text{ cm}^{-3}$. This observation shall not be discussed quantitatively in the following; however, it is conceivable that as an increase in the ^{31}P doping concen-

tration leads to a smaller main-pair distance (note the definition of main-pair distance given in Sec. IV A 2) for ^{31}P to interface-defect pairs as well as ^{31}P to ^{31}P pairs, it should not lead to a change in the main-pair distance of interface-defect pairs. The observed general decrease in the transition time with an increase in the ^{31}P concentration therefore suggests that the observed signals are predominantly due to transitions involving ^{31}P and not transitions between two interface defects. We note that there may be other reasons for this decrease in transition times with increasing doping density: one such possibility is that different internal fields may lead to different energy separations between pair partners with different intrapair distance, with a corresponding change in transition probability.

(iii) The entire set of data reveals a strong correlation of τ_0 between any combinations of signals, whether it is between the two ^{31}P hyperfine signals or between the interface signals and either one of the two ^{31}P hyperfine signals. The correlation between the two ^{31}P hyperfine peaks is expected as the only difference between ^{31}P atoms contributing to these two peaks is the nuclear-spin state, which has little influence on electronic transitions times. The strong correlation between the ^{31}P peaks and the interface states is again strong evidence that the spin-dependent transitions measured involve ^{31}P interface-defect pairs in the way sketched in Fig. 1(b).

It was not possible to obtain unambiguous correlation plots similar to those in Fig. 4 for the two different interface and near-interface defects discussed above. It is therefore not possible to verify whether the observed correlation between the ^{31}P and the interface defects applies to both interface centers or only to the one which dominated under the observed conditions. However, we point out that the strong correlation seen in the plots of Fig. 4 is consistent with the assumption that the dynamics of both defects correlates with the ^{31}P dynamics and, thus, spin-dependent recombination through both interface defects in the manner sketched in Fig. 1(b) seems to be possible.

The correlation data in Fig. 4 raise a question about the presence of spin-dependent transitions between interface defects. It is known from previous pEDMR studies of (111) oriented nominally intrinsic *c*-Si/SiO₂ interfaces at X band,²⁹⁻³¹ as well as from recent pEDMR studies at high magnetic fields (≈ 8.5 T) (Ref. 28) that spin-dependent transitions involving only interface defects but not ^{31}P are possible and that these transitions can be due to spin-dependent resonant tunneling between two interface states in sufficient spatial and energetic proximity. We conclude from the data seen in Fig. 4 that, while such interface-defect-only processes may or may not have been present at the investigated *c*-Si:P/SiO₂ interfaces, they did not dominate the observed spin-dependent rates, consistent with the very weak signal strength of previous pEDMR measurements on intrinsic *c*-Si/SiO₂ interfaces conducted at X band.³¹ The interface-defect signals are weak in spite of the presence of a significantly higher interface-defect density compared to the areal density of ^{31}P close to the interface. This may be explained by considering the signal from interface-defect pairs, which have almost identical *g* factors and therefore stronger coupling, leading to lower pEDMR signals than those seen from

^{31}P -defect pairs which have quite different *g* factors and weaker, but still finite, coupling,⁴² and therefore dominate the signal. Another possibility that could account for the weakness interface-interface transitions is simply the significantly smaller geometrical size of the interface states in comparison to the large ^{31}P donor wave function which extends over several nm.

D. Electrical detection of spin coherence

1. Experimental data

The ability to perform spin-Rabi nutation is a crucial prerequisite for the coherence time measurements using echo pulse sequences as it reveals the resonantly induced Rabi frequency for a given set of experimental conditions (e.g., for the applied microwave power). The Rabi frequency is needed to determine the pulse lengths required to obtain the correct nutation angles during the pulse sequences. We performed transient nutation style experiments for the electrical detection of spin-Rabi nutation. For these measurements, the photocurrent change ΔI was integrated between two appropriately chosen integration times t_1 and t_2 after the microwave pulse, so we obtain a charge

$$Q = \int_{t_1}^{t_2} \Delta I(t) dt \quad (1)$$

that is proportional to the number of spin-dependent transitions induced by the resonant excitation.⁴² As Q is proportional to the projection of the resonantly prepared coherent spin state $|\psi(\tau)\rangle$ at the end of the excitation pulse of length τ onto the singlet state $|S\rangle$,^{10,40} the measurement of $Q(\tau) \propto |\langle S|\psi(\tau)\rangle|^2$ reveals the propagation of the singlet content of $|\psi(\tau)\rangle$ during the pulse in a transient nutation-style experiment. Figure 5(a) displays the measurement of $Q(\tau, B_0)$ as a function of the pulse length τ and the magnetic field B_0 for a *c*-Si sample with $[\text{P}] = 10^{16} \text{ cm}^{-3}$, a temperature $T = 5$ K, $\theta = 90^\circ$, and integration times $t_1 = 6 \mu\text{s}$ and $t_2 = 16 \mu\text{s}$.

2. Discussion

The data set displayed in Fig. 5 shows that $Q(\tau)$ has an oscillating behavior around the same magnetic fields which produced local current response maxima in the data set displayed in Fig. 2. The oscillatory dependence on τ is due to the dephasing spin-Rabi nutations as demonstrated, for the magnetic field $B_0 = 348$ mT, by the data sets displayed in Fig. 5(b): the four plots show $Q(\tau)$ for four different microwave powers (B_1 field strengths). We anticipate⁴⁰ the spin-Rabi-nutation signal of an inhomogeneously broadened spin ensemble to follow the integral of a first kind Bessel function,

$$Q(\tau) \propto \int_0^{\gamma B_1 \tau} J_0(2x) dx = \frac{1}{\pi} \int_{-\infty}^{\infty} \frac{\sin^2(\gamma B_1 \tau \sqrt{1+x^2})}{1+x^2} dx, \quad (2)$$

in which $\gamma \approx 2.8$ MHz/G is the gyromagnetic ratio. A fit of the four data sets in Fig. 5(b) with Eq. (2) shows a good

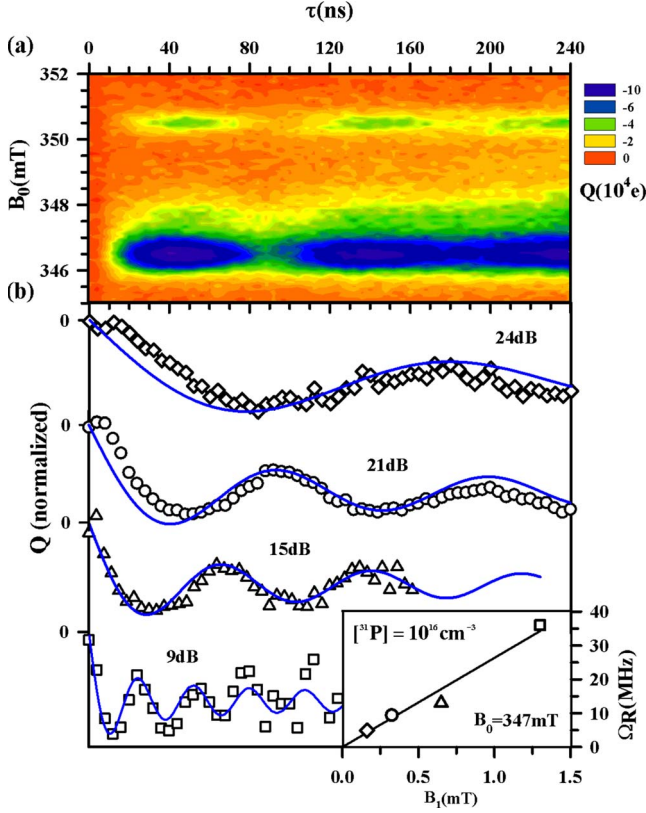


FIG. 5. (Color online) (a) Plot of the measured integrated charge $Q(\tau, B_0)$ as defined by Eq. (1) as a function of the magnetic field B_0 and the length τ of an applied microwave pulse with frequency $f = 9.7475$ GHz and power $P = 8$ W. (b) The symbols represent a plot of the measured charge $Q(\tau)$ for four different microwave powers at $B_0 = 347$ mT. Note that for the latter case, the pulse length was recorded up to $\tau = 120$ ns only as the measurement was limited by signal perturbation due to the pulse induced microwave current artifacts. The blue lines represent fits of an integrated Bessel function to the experimental data. The Rabi-nutation frequencies obtained from these fits are displayed in the inset as a function of the applied B_1 field. The fit of a linear function through the origin (black line) shows good agreement.

agreement and provides values for the nutation frequencies $\Omega_R = \gamma B_1$ for the four different powers. A plot of Ω_R versus the B_1 fields obtained from the relative microwave attenuation used for the four measurements shows that the expected linearity of the spin-Rabi nutation is given. The data in Fig. 5 are thus shown to be due to the spin-Rabi nutation of ^{31}P donor and interface electron spins, confirming the previously reported observation made for $c\text{-Si}(100)\text{:P/SiO}_2$ interface with higher ^{31}P concentration. Note that with the data obtained from the transient nutation measurement, it is possible to determine the length of π and $\frac{\pi}{2}$ pulses as needed for the T_2 measurements in the following. The latter will be necessary since the decay of the Rabi nutation as displayed in Fig. 5 is not a measure for spin coherence. The agreement of the nutation data with the integrated Bessel function is indicative of coherent dephasing, not coherence decay, being the dominant source of the observed nutation decay. This assumption is confirmed by the electrically and pEPR detected echo data discussed below, which shows that the real T_2 spin-

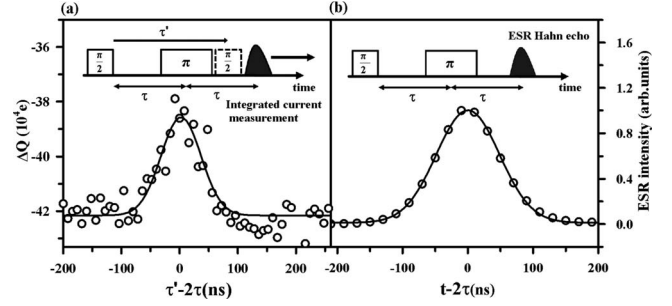


FIG. 6. Comparison of (a) an electrically detected spin echo with $\tau = 300$ ns and (b) a conventional microwave detected Hahn echo with $\tau = 10$ μs . The data sets were recorded on the same sample, under identical sample conditions ($T = 10$ K, $I = 250$ μA , and $\theta = 90^\circ$) during the same experimental run on resonance with the low-field phosphorous line. Both data sets were fit with Gaussian functions (solid line). Insets of the two plots show sketched timelines of the used pulse sequences.

coherence time of the ^{31}P donor electrons is significantly longer than the decay of the nutation signal.

E. Comparison of the coherence time T_2 of ^{31}P donor electrons at the $c\text{-Si:P/SiO}_2$ interface and in the $c\text{-Si:P}$ bulk

1. PEDMR and pEPR detected spin echoes

The data presented in Secs. IV A and IV C showed that the spin-dependent current observed at $c\text{-Si:P/SiO}_2$ interfaces are due to transitions that take place between ^{31}P donor electron states and $c\text{-Si:P/SiO}_2$ interface states in their proximity. A measurement of the ^{31}P donor electron-spin-coherence time (the T_2 time) using pEDMR will therefore reveal only T_2 of ^{31}P donor electrons in close proximity to the $c\text{-Si:P/SiO}_2$ interface defects. In contrast, a T_2 measurement using conventional microwave detected pEPR will reveal the coherence time of ^{31}P donors in the bulk as the contribution of near-surface ^{31}P atoms in the pEPR signal will be negligible in comparison to the magnitude of the bulk ^{31}P signal. Thus, the comparison of T_2 times measured by pEDMR and pEPR allows the influence of interface defects on the ^{31}P donor electron-spin-coherence times to be studied.

It shall be noted that, in the following, the constant T_2 is used for all decay time measurements of Hahn-echo decays as the pEPR detected Hahn-echo decays represent the transverse relaxation T_2 for the bulk donor electrons. It must be emphasized though that the nature of the observed transition may be of completely different physical origin than transverse spin relaxation and the identification of the nature of this process is the motivation for these experiments.

The pEPR and pEDMR experiments require different approaches to the measurement of T_2 times: with pEPR, the T_2 times of paramagnetic centers can be determined most easily using a Hahn-echo pulse sequence.⁴⁵ Hahn echoes are a temporary rephasing of a spin ensemble due to a pulse sequence consisting of an initial $\pi/2$ pulse which turns the ensemble polarization into the plane perpendicular to the B_0 field and a subsequent π pulse which initiates the phase reversal.⁴⁶ As illustrated in the inset sketch in Fig. 6(b), when the echo

pulse sequence consists of the $\frac{\pi}{2}-\pi$ pulses with a duration τ between the pulses, a Hahn echo can be observed at a time τ after the second pulse, which is the time 2τ after the first pulse. When a Hahn echo is observed, T_2 times can be measured by determining the decay of the Hahn echo as a function of twice the pulse separation time 2τ . Figure 6(b) shows a data set for a Hahn-echo transient obtained from a ^{31}P -doped *c*-Si sample with $[^{31}\text{P}]=10^{16}\text{ cm}^{-3}$ at a temperature $T=10\text{ K}$ and with $\theta=90^\circ$. One can clearly see a local maximum of the transient microwave signal at a time $t=2\tau$. The data set was well fit by a Gaussian function with a half width of $\sigma=24.4(2)\text{ ns}$. In the following, Gaussian fits are used to determine the integrated intensities of all pEPR and pEDMR detected Hahn echoes.

In contrast to pEPR measurements, pEDMR does not allow direct observation of Hahn-spin echoes through real-time transient measurements as the integrated sample current $Q(\tau)$ always represents a projection of the spin state at the end of the pulse sequence onto a singlet state. Therefore, the T_2 time measurement using pEDMR requires the utilization of a modified Hahn-echo pulse sequence that is illustrated in the inset of Fig. 6(a).⁶ In order to resolve the dynamics of the spin ensemble during and after the $\frac{\pi}{2}-\pi$ pulse sequence, a third pulse with length $\frac{\pi}{2}$ is applied at a time τ' after the beginning of a conventional Hahn-echo pulse sequence. The third pulse projects the spin ensemble at the time τ' onto the \hat{z} direction, which in turn determines the singlet content of the ^{31}P interface-defect pair. The charge Q integrated following this pulse therefore represents the polarization of the spin ensemble along the \hat{x} axis (\hat{y} axis) at the time τ' [assuming the B_1 field is directed along the \hat{y} axis (\hat{x} axis)]. The measurement of the entire echo transient using the pEDMR detection requires repetition of the echo sequence for various τ' : the third pulse (also called the detection pulse) is swept through the time range which covers the Hahn-echo maximum as well as the echo base line. While this procedure makes the time needed for T_2 measurements significantly longer, it allows the measurement of a T_2 using pEDMR. The plot displayed in Fig. 6(a) shows an electrically detected spin echo measured on the same sample and under identical conditions, recorded during the same experimental run as the measurements shown in Fig. 6(b). The data clearly show the echo whose fit with a Gaussian function is displayed by the solid line. The fit revealed a half width of $\sigma=19(2)\text{ ns}$. The comparison of the two echo functions shows that the electrically detected echo is narrower than the microwave detected echo, indicating that the former is due to a more heterogeneous spin ensemble.

The use of two different measurement techniques (pEDMR and pEPR) raises the question of whether both methods probe the same observable, namely, T_2 of ^{31}P impurity atoms. There has recently been a comparative study of T_2 times confirming this identity using a pEDMR detected spin-dependent bulk process³⁷ (a spin-trap process of ^{31}P in *c*-Si that becomes relevant at high magnetic fields) which showed that both pEDMR and pEPR measured T_2 times reveal an excellent agreement. Thus, in the following, systematic measurements comparing pEPR detected T_2 times of ^{31}P bulk impurities and pEDMR detected T_2 times of ^{31}P inter-

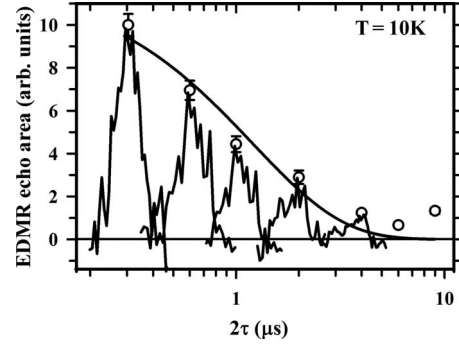


FIG. 7. Plot of integrated intensities of the electrically detected echoes as a function of 2τ recorded with pEDMR on a *c*-Si:P/SiO₂ sample with $[\text{P}]=10^{16}\text{ cm}^{-3}$ on resonance with the low-field phosphorous line. The solid line represents a fit with a modified multi-exponential decay function (see text); the small inset plots represent plots of echo data sets.

face impurities are presented. These measurements are made for three reasons: (i) to extend the previous observation of electrically detected Hahn echoes⁶ to *c*-Si(111) surfaces, (ii) to measure the temperature dependence of the T_2 times, and (iii) to obtain comparable measurements with both pEPR and pEDMR under identical conditions but with completely different detection channels.

2. Measurement of spin-echo decays

The spin-echo effects shown in Fig. 6 are imprints of coherent spin motion on currents or radiation intensities. When a spin ensemble loses coherence during a $\frac{\pi}{2}-\pi$ sequence, the intensity of the spin echo following this sequence decays. Quantifying the decay of Hahn echoes is a direct measure of the coherence time T_2 .⁴⁶ Figure 7 displays a set of electrically detected Hahn echoes as well as a plot of the integrated echo intensities obtained from them, recorded on a sample with $[\text{P}]=10^{16}\text{ cm}^{-3}$ at magnetic fields in resonance with the high-field ^{31}P peak at $T=10\text{ K}$ and $\theta=90^\circ$, and with a sample current of $I=250\text{ }\mu\text{A}$. One can clearly see the gradual decay of the echo intensity with increasing pulse separation time τ . The solid line of the plot in Fig. 7 displays a fit of the intensity data with a modified exponential function

$$I(2\tau) = e^{-(2\pi T_2) - (8\tau^3/T_S^3)}, \quad (3)$$

which contains a contribution due to a single exponential T_2 decay as well as the stretched exponential contribution due to the isotopical influence of the ^{29}Si , which causes spin diffusion with time constant T_S .^{7,37} The plot in Fig. 7 exhibits a good agreement of the echo decay with the fit function and thus, by using this method for both pEDMR as well as pEPR detected echo decay measurements, the T_2 times of ^{31}P impurities can be determined for the *c*-Si:P bulk and the *c*-Si:P/SiO₂ interface, respectively. Note that all pESR detected and most pEDMR detected echo measurements were conducted on the low-field peak of the hyperfine split ^{31}P resonance. In order to confirm that the spectral proximity of the P_b peak to the low-field ^{31}P resonance under the given

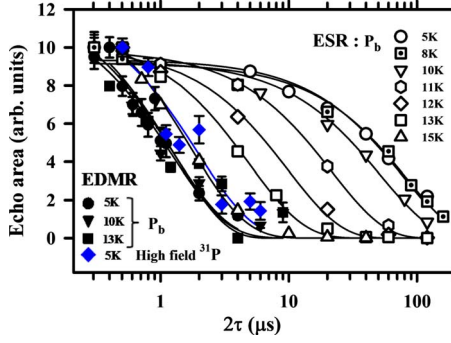


FIG. 8. (Color online) Plot of the normalized integrated echo intensity of pEPR and pEDMR detected Hahn echoes as a function of the pulse separation time 2τ for various temperatures. The data sets were fit with the modified exponential function given by Eq. (3). All pEDMR and pEPR measurements were conducted on the same samples during the sample experimental run. Most of the data points were recorded on resonance with the low-field phosphorous line except for the blue colored data points which were recorded on resonance with the low-field phosphorous line.

experimental conditions does not distort the electrical T_2 measurements, control measurements were carried out on the high-field ^{31}P peak for $T=5$ K. The values obtained under these conditions are $T_2=1.2(3)$ μs for the low-field peak and $T_2=1.9(8)$ μs for the high-field peak. Within the given error margins, the results of these control measurements (blue solid diamonds in Fig. 8) are in agreement with the measurements obtained from the low-field ^{31}P resonance and, also, they are in good agreement with the measurements conducted at *c*-Si(100) surfaces⁶ which had been treated in a similar manner (native oxide).

3. Temperature dependence of T_2 times

The measurement of T_2 as described above was repeated for the low-field resonance on the same sample with pEPR at temperatures of $T=5, 8, 10, 11, 12, 13,$ and 15 K and with pEDMR at temperatures of $T=5, 10,$ and 13 K. The integrated echo intensities of these measurements are plotted in Fig. 8 along with the results of their fit with Eq. (3). The comparison of the pEDMR and the pEPR data sets shows that while there is a strong temperature dependence of the echo decay for the pEPR data, the pEDMR decay is faster and, within the range $T=5$ – 13 K, nearly constant. In order to analyze these observations quantitatively, the fit results for T_2 are plotted for both the pEDMR and the pEPR measurements in an Arrhenius plot in Fig. 9.

The coherence time of the bulk ^{31}P donors, T_2 , determined via pEPR, is well fit with a function of the form

$$\frac{1}{T_2} = A e^{-\Delta E/k_B T} + \frac{1}{T_0}, \quad (4)$$

where ΔE is an activation energy and $1/T_0$ is a constant relaxation rate independent of temperature. The best fit occurs with $\Delta E=9.1 \pm 0.5$ meV and $1/T_0=10 \pm 1$ kHz.

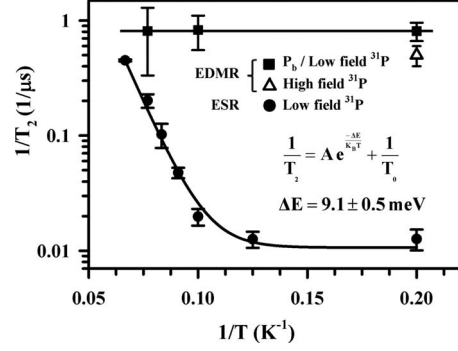


FIG. 9. Plot of the logarithm of coherence decay rate T_2^{-1} obtained from the data shown in Fig. 8 as a function of the inverse temperature T^{-1} . The solid lines are fits of the data. The pEDMR data are fit with a constant function. The pEPR is fit with a combination of a constant function and a temperature activated Boltzmann factor.

4. Discussion

As the pEDMR and the pEPR data displayed in Fig. 9 were collected on the same sample in the same experimental run, it is clear that the pEDMR measured T_2 times of ^{31}P donor spins in close proximity to interface defects are significantly shorter than the pEPR measured T_2 times and, within the error, independent of the temperature. At the same time, the pEPR measured T_2 of the bulk ^{31}P donor spins is not only longer than the pEDMR measured ^{31}P donor spins, but it is also highly temperature dependent. In the temperature range from $T=5$ to 15 K, the coherence time changes by about a factor of 50, exhibiting a good agreement with the previously demonstrated thermal activation⁷ of ^{31}P in a *c*-Si environment with a natural abundance of the ^{29}Si isotope. The comparison of T_2 of ^{31}P in proximity to interface defects with those in the bulk therefore shows that interface defects significantly shorten the donor electron-spin-coherence time. Within the given temperature range, T_2 appear to be pinned at ≈ 1.3 μs , a value which has been observed previously for electrically detected ^{31}P spins in *c*-Si samples with different surface orientations, donor concentrations, and experimental conditions.^{6,10} The independence of the donor spin-coherence time of near-interface-defect ^{31}P atoms from experimental conditions, including temperature, suggests that in contrast to bulk donors, T_2 of the near-surface donors is not determined by (^{31}P - ^{31}P) spin-spin or spin-lattice interactions but by processes directly related to the interface defects in their immediate proximity.

We identify two possible origins for the drastic quenching of the ^{31}P donor electron-spin T_2 time in proximity to interface defects described above:

(i) The electronic transition between the ^{31}P donor state and the P_b center. This occurs when the donor electron falls into the doubly occupied interface ground state. The electronic transition leaves both the ^{31}P donor and the interface state diamagnetic since there is no donor spin present after the transition and the interface state is a doubly occupied singlet state.

(ii) Spin flip-flops of interface states which significantly quench the T_2 relaxation of ^{31}P donor spins in their proximity, as suggested by de Sousa.¹⁵

TABLE I. Expectation for the observed time constants in electrically detected inversion recovery and Hahn-echo experiments for a number of different relationships between the T_1 , T_2 , and electronic transition times, T_{elec} . We note that, in the main text, the experimentally determined times are referred to as T_1 and T_2 , respectively, even when they may be due to electronic transitions.

Relationship	^{31}P		Low-field P_b	
	Inversion recovery	Hahn echo	Inversion recovery	Hahn echo
$T_{\text{elec}} \ll T_2^{31\text{P}}, T_2^{\text{P}_b} \ll T_1^{31\text{P}}, T_1^{\text{P}_b}$	T_{elec}	T_{elec}	T_{elec}	T_{elec}
$T_2^{31\text{P}}, T_2^{\text{P}_b} \ll T_{\text{elec}} \ll T_1^{31\text{P}}, T_1^{\text{P}_b}$	T_{elec}	$T_2^{31\text{P}}$	T_{elec}	$T_2^{\text{P}_b}$
$T_2^{31\text{P}}, T_2^{\text{P}_b} \ll T_1^{31\text{P}}, T_1^{\text{P}_b} \ll T_{\text{elec}}$	$\frac{T_1^{31\text{P}}T_1^{\text{P}_b}}{T_1^{31\text{P}}+T_1^{\text{P}_b}}$	$T_2^{31\text{P}}$	$\frac{T_1^{31\text{P}}T_1^{\text{P}_b}}{T_1^{31\text{P}}+T_1^{\text{P}_b}}$	$T_2^{\text{P}_b}$

The electronic transition is a limitation to both T_1 as well as T_2 processes of the spin pairs as it destroys the pairs. When the electronic transition determines the measured T_2 times, both the electrically measured T_2 and T_1 times should be equal. This is in contrast to the general case of spin relaxation in the absence of electronic transitions when $T_2 \leq 2T_1$ and also in contrast to the case when the interface state induced enhancement of the ^{31}P T_2 relaxation keeps T_1 either unchanged or significantly slower than the T_2 time. In this latter scenario, the electronic transition time will be longer than the P_b induced T_2 time and, thus, the electrically measured T_1 time will be given by either the real T_1 time or the electronic transition time and it should therefore be significantly longer than the electrically measured T_2 times.

For clarity, Table I shows the expected measurement outcomes for electrically detected Hahn-echo and inversion recovery experiments, for a number of different relationships between the underlying T_1 , T_2 , and electronic transition times T_{elec} . Note that the term “electronic transition time” used here refers to the singlet transition probability. Since the permutation symmetry of the resonantly excited pairs shuttles back and forth between singlet and triplet states during Rabi-nutation experiments (and, thus, during both Hahn-echo and inversion recovery experiments), it is the dominating singlet transition, not the slow triplet transition, which determines the measured decay times when electronic transition times are shorter than any spin relaxation time.

F. Comparison of T_2 and the longitudinal relaxation time T_1 of ^{31}P donor electrons at the $c\text{-Si:P/SiO}_2$ interface

1. Electrical detection of spin inversion

In order to probe T_1 of near-interface ^{31}P , electrically detected inversion recovery experiments were carried out at a temperature of $T=5$ K, where pESR measurements of bulk ^{31}P donor spins reveal large differences between T_1 and T_2 times.⁷ The idea behind the inversion recovery experiment⁴⁶ is to invert the steady-state spin polarization and to then observe transiently the gradual return toward the equilibrium due to T_1 processes. Thus, the experiment consists of an initial inversion pulse, a defined delay time τ'' during which the spin ensemble undergoes T_1 relaxation, and a subsequent polarization measurement, which is typically conducted by

the utilization of a Hahn-echo sequence with a fixed pulse separation time τ . Figure 10 displays a sketch of the pulse sequence used for the electrical inversion recovery measurements presented in the following. Similar to the Hahn-echo decay measurements, the Hahn echo is measured with pEDMR by repetition of the experiment while applying projection pulses which are gradually swept through the echo sequence. The data in Fig. 10 show an inverted Hahn echo recorded with a short $\tau=252$ ns and an even shorter delay time $\tau''=52$ ns producing strong inversion. The experimental data were collected at a B_0 field in resonance with the high-field ^{31}P line, which is well separated from the P_b resonances. It shows that in contrast to the positive spin echo as detected for a simple Hahn-echo sequence, the sign of the echo is negative. The data shown in Fig. 10 are a demonstration of an electrically detected spin inversion experiment.

Similar to the T_2 times discussed above, the variable T_1 is used in the following for all recovery times of inversion recovery experiments since the pEPR detected inversion recovery of the bulk donor electrons represents the longitudinal

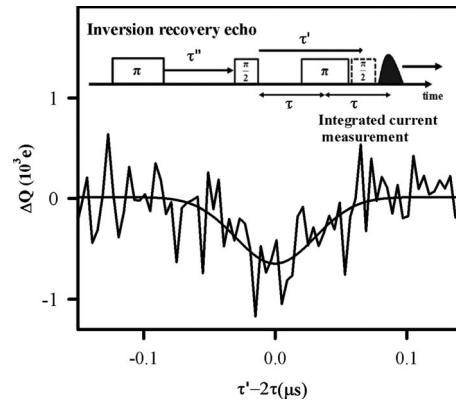


FIG. 10. Demonstration of an electrically detected spin inversion recovery experiment. The inset is a sketch of the inversion recovery pulse sequence which consists of the Hahn-echo sequence that is preceded by an inversion (π) pulse at a time τ'' before the Hahn-echo sequence begins. Similar to the electrically detected Hahn echo shown in Fig. 6, a projection pulse is shifted through the sequence during different repetitions of the experiment. The main plot displays an echo recorded by plotting Q as a function of the difference $\tau' - 2\tau$ between the projection pulse begin τ' and the echo maximum at 2τ .

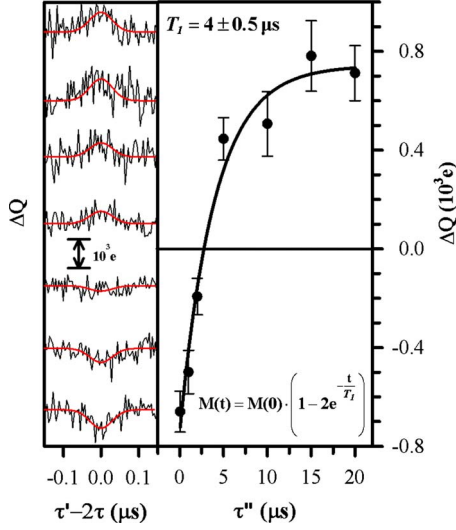


FIG. 11. (Color online) Plot of the integrated echo intensity detected with the pulse sequence shown in Fig. 10 as a function of the inversion recovery time τ'' . The solid line represents a fit of the data with a single exponential function. Note that the inverted echo for small τ'' changes into a noninverted echo with equal magnitude for large τ'' . The inset plots on the left show the raw data of the various echo measurements as well as fits with Gaussian functions which are the basis for the integrated echo intensities.

relaxation time T_1 . It is important to note that by using this notation for the pEDMR detected inversion recovery times, T_1 may actually quantify a process of completely different physical origin than longitudinal relaxation, such as the electronic transition between the phosphorous and the interface defect. The possible relationship between the measured times and the underlying processes are summarized in Table I.

2. Inversion recovery of near-interface-defect ^{31}P donor electrons

In order to determine the T_1 times of the ^{31}P donor electron, the experiment shown in Fig. 10 was repeated for seven values of τ'' in the range of $52 \text{ ns} \leq \tau'' \leq 20 \text{ } \mu\text{s}$. The results of these experiments are displayed in Fig. 11. They show that the polarization inversion that exists directly after the inversion pulse (τ'' is very small) exponentially approaches the steady-state polarization with increasing τ'' . The integrated echo amplitudes were obtained from a fit of the echo data with Gaussian functions. Their dependence on τ'' shows an excellent agreement with an exponential decay function with a negative offset

$$M(\tau'') = M(0)[1 - 2e^{-\tau''/T_1}]. \quad (5)$$

The time constant $T_1 = 4.0(5) \text{ } \mu\text{s}$ obtained from this fit is more than six orders of magnitude shorter than the previously investigated bulk T_1 times,⁷ which shows that the proximity to P_b centers leads to dramatically reduced T_1 times.

3. Discussion

The measurement of $T_1 = 4.0(5) \text{ } \mu\text{s}$ of ^{31}P donor electrons in proximity to interface defects reveals a value that is

quenched by orders of magnitude compared to bulk ^{31}P T_1 times. It can therefore be concluded that the measured T_1 of ^{31}P donor electrons near interface state times is governed not by the same T_1 processes that act on bulk donor electrons but instead by the spin-dependent ^{31}P - P_b transition.

The electrically detected T_1 time is longer than the electrically detected T_2 times for the two ^{31}P resonance peaks that were measured at a temperature of $T = 5 \text{ K}$. Note that the EDMR signal of the low-field ^{31}P peak overlaps with interface-defect signals, which explains why its value of $T_2 = 1.2(3) \text{ } \mu\text{s}$ differs from the high-field ^{31}P which shows $T_2 = 1.9(8) \text{ } \mu\text{s}$. The differences between T_1 times and the two T_2 values reveals $2.8(6)$ and $2.1(9) \text{ } \mu\text{s}$, for the low- and high-field ^{31}P resonances, respectively. Thus, while it is likely that $T_2 < T_1$, there is only limited statistical support for the measured difference between the T_1 and T_2 times.

G. Comparison of T_2 and T_1 times at different interface-defect densities and different pair partner resonances

In order to corroborate the observation that electrically detected ^{31}P donor electron relaxation times $T_2 < T_1$, and that T_1 and T_2 are independent, electrically detected Hahn-echo decay and inversion recovery experiments were repeated on the high- and low-field resonance lines of the ^{31}P donor electrons on a sample with a different interface-defect density.

1. Testing the independence of T_1 and T_2 relaxation times

In order to test the conclusions given in Sec. IV F 3, the Hahn-echo and inversion recovery experiments presented above were repeated on a sample with identical ^{31}P density ($[^{31}\text{P}] = 10^{16} \text{ cm}^{-3}$) but reduced interface-defect density. This was accomplished by preparing the pEDMR sample in an identical way to the sample used for the measurements in Sec. IV F, followed by a thermal anneal at $T = 500 \text{ K}$. It is well known¹⁶ that the thermal activation of $c\text{-Si/SiO}_2$ interface leads to a structural relaxation, which greatly reduces the number of interface states. Based on the parameters used,⁴⁷ we estimate a reduction in the interface state density by a factor of 4, thus increasing the average distance between interface defects by a factor of 2.

Two outcomes of this decrease in defect density are anticipated. First, the increased separation between defects may lead to an increase in the defect T_1 time. Second, the decreasing defect density should also increase the main-pair distance (as defined in Sec. IV A 2) monotonically (but nonlinearly). As this would reduce the transition times between the ^{31}P donor and the interface defect, we expect the electrically detected T_1 time to increase if they are determined by the transition time. In both cases, we expect the T_1 time measured using an electrically detected inversion recovery experiment to increase when the defect density is reduced. We do not, however, expect to increase the measured T_2 times in the same way if they are dominated by the local interface fields. In contrast, when T_2 is mostly governed by the electronic transition, it is expected to follow the changes in the T_1 times.

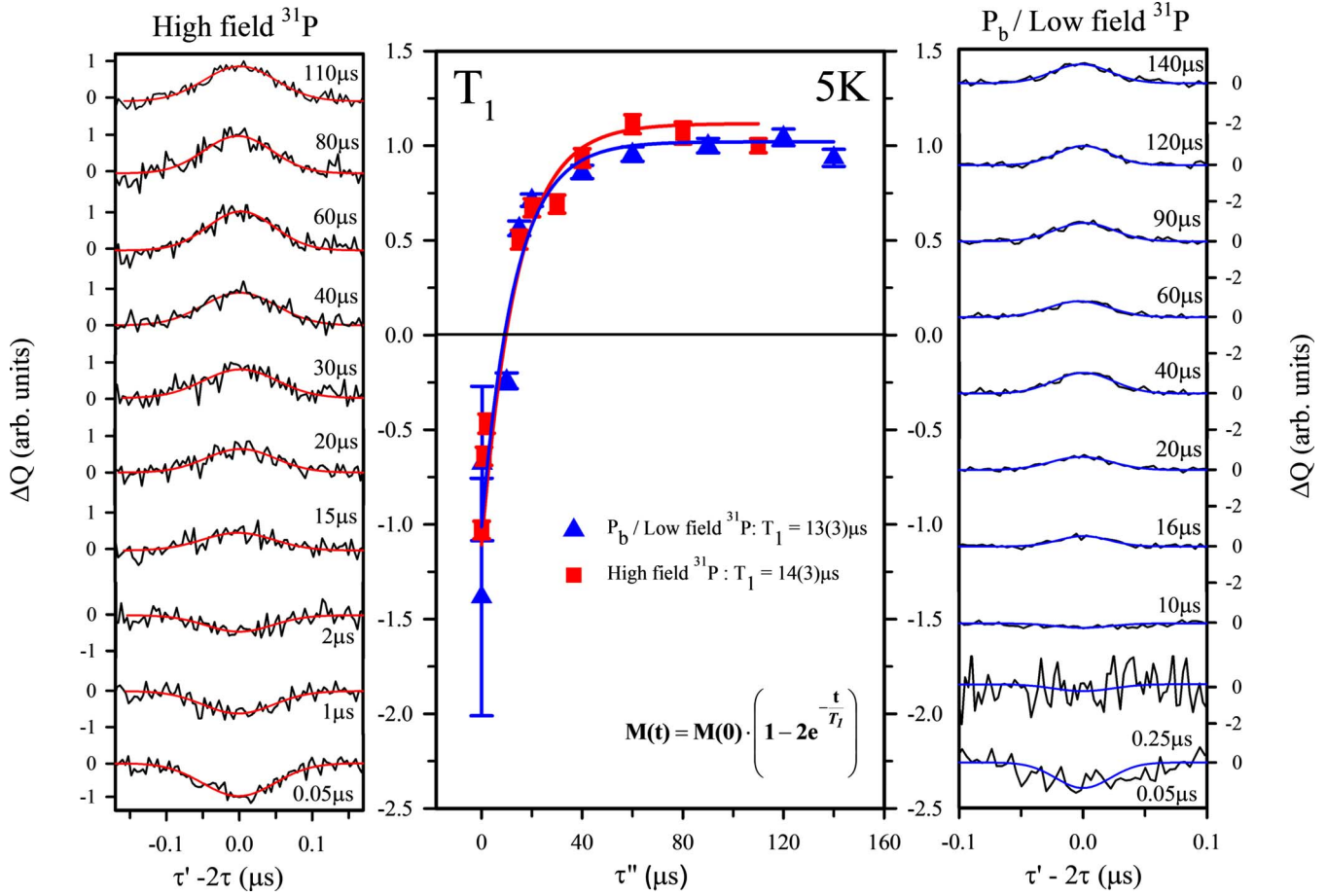


FIG. 12. (Color online) Electrically detected inversion recovery measurements of electron spins on the low-field $^{31}\text{P}/\text{P}_b$ resonance and the high-field ^{31}P resonance measured on an annealed sample at $T=5$ K. The values of τ' are listed next to the plotted echoes. The data are normalized to the echo measured with large τ' . Within the given error ranges the two data inversion recovery plots show similar T_1 times. These T_1 times are increased in comparison to the T_1 time of the nonannealed sample.

Figure 12 displays the results of pEDMR detected inversion recovery experiments measured on both the ^{31}P high- and low-field and P_b resonances of the annealed sample. The data are plotted on integrated echo intensity scales which are normalized to the noninverted Hahn echoes (for large τ'). As for the data in Fig. 11, the integrated echo intensities were determined using a Gaussian fit. Because the low-field ^{31}P and the P_b signals overlap, the low-field $^{31}\text{P}/\text{P}_b$ echo signals have different signal strengths and thus different relative noise levels exist for the two resonances. The plots of the echo intensity as a function of the inversion time τ' confirms again the presence of an inverted signal directly after the inversion pulse, which gradually changes into a noninverted Hahn echo as τ' is increased. The two measurements reveal echo inversion times of $T_1=13.3(3) \mu\text{s}$ and $T_1=14.3(3) \mu\text{s}$ for the low- and high-field signals, respectively. In spite of the fact that the low-field measurements included contributions from the ^{31}P and the P_b signals, both measurements are within two standard deviations [the difference is $1.0(5) \mu\text{s}$] and at the same time they are significantly longer than the T_1 times measured on the nonannealed sample as expected for an interface with a reduced density of interface states.

In order to compare the T_1 times and the T_2 times of the annealed sample, we conducted Hahn-echo decay measure-

ments on both ^{31}P resonances. In contrast to the T_1 measurements, these echo decays were measured at various temperatures between $T=5$ and 12 K. The echo decay functions were fit with the same procedure used for the nonannealed sample (see Sec. IV E 2). The results of these fits are plotted in Fig. 13. For the low-field $^{31}\text{P}/\text{P}_b$ resonance they confirm the observations made on a native oxide qualitatively and

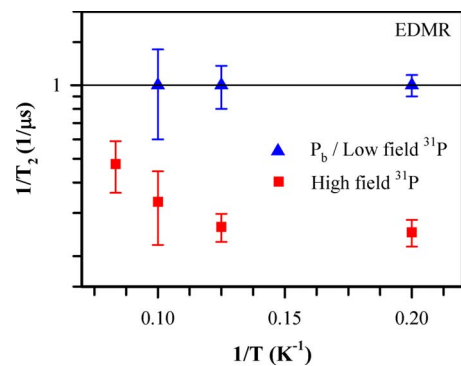


FIG. 13. (Color online) The results of electrically detected Hahn-echo decay measurements of electrons spins at on the low-field $^{31}\text{P}/\text{P}_b$ resonance and the high-field ^{31}P resonance measured on an annealed sample at temperature between $T=5$ and 12 K.

TABLE II. PEDMR detected inversion recovery times (T_1) and Hahn-echo decay times (T_2) recorded on the high- and low-field resonances at a temperature $T=5$ K for both the nonannealed (native) and the annealed silicon to silicon dioxide interfaces.

Resonance line	High-field ^{31}P		Low-field $^{31}\text{P}/\text{P}_b$	
	Native (μs)	Annealed (μs)	Native (μs)	Annealed (μs)
Interface condition				
pEDMR T_1	4.0(5)	14(3)		13(3)
pEDMR T_2	1.9(8)	4.0(5)	1.2(3)	1.0(2)

quantitatively—the value of T_2 is independent of the temperature at $\approx 1 \mu\text{s}$. The measurements also confirm that T_2 measured solely on ^{31}P (by measuring on the high-field resonance) is increased and, due to the improved relative errors, one can state that it is significantly longer than the value measured on the high-field $^{31}\text{P}/\text{P}_b$ peak and significantly shorter than the measured T_1 time. The high-field ^{31}P T_2 time also remains constant between $T=5$ and 8 K. At higher temperatures its value decreases, as seen in conventional pESR experiments.⁷

2. Discussion

Table II summarizes the results of T_1 and T_2 measurements for both the low-field $^{31}\text{P}/\text{P}_b$ and high-field ^{31}P resonances, for the two different interfaces, at a temperature of $T=5$ K. The measurements made on the annealed sample confirm qualitatively the behavior of T_1 and T_2 times obtained from the nonannealed sample: the T_2 times of ^{31}P donor electrons near interface defects are significantly shorter than the T_2 times of ^{31}P donor electrons in the bulk.

The identical measured T_1 times seen for both ^{31}P and P_b may be explained in two ways, as can be seen from Table I. In one case, the electronic transition may be much faster than the underlying T_1 process. Here, the electronic transition time T_{elec} determines the measured T_1 time and corresponds to the faster of the two spin-pair decay times, namely, the singlet electronic transition. An alternate explanation is that one (or both) of the pair partners has an underlying T_1 time faster than the electronic process. In that case, the electrically detected inversion recovery measurement will reflect that time for experiments undertaken on *either* partner, as we measure the relative orientation of the two spins, and not the absolute orientation observed in conventional ESR experiments. Indeed, T_1 times measured in any pair system using the electrically detected inversion recovery method described here should always result identical T_1 times for both pair partners. We are thus unable to distinguish the underlying cause of the measured reduction in the ^{31}P T_1 time—it may be due to a real reduction in the T_1 time due to its environment, the intrinsic T_1 of the partner P_b spin, or the electronic transition between them. We note that, if the electrically measured T_1 and T_2 times had been identical, we would be confident that the electronic transition was the dominant mechanism.

V. CONCLUSIONS

The data presented and discussed above strongly support the model for spin-dependent recombination via ^{31}P donors

and interface defects that were presented by Stegner *et al.*¹⁰ While this explanation for the observed EDMR signal has become commonly accepted, and is further supported by the results presented here, the possibility remains that other processes also contribute to the resonant changes in current. Given the now significant evidence supporting the $^{31}\text{P}-\text{P}_b$ model,^{6,10,27} we agree with the conventional understanding and conclude here that we are indeed observing spin-dependent transitions between ^{31}P donors located close to P_b defects at the Si(111)- SiO_2 interface.

The measurement of the T_2 times of ^{31}P near $c\text{-Si}/\text{SiO}_2$ interface defects with electrically detected echo decay experiments shows that the T_2 times of the two weakly spin coupled pair partners are significantly different, and that both are significantly shorter than the T_1 times. We conclude from this observation that the measured T_2 times of the P_b center and the ^{31}P donor electron are not primarily governed by the electronic transition and that due to the weak spin coupling, the transverse spin relaxations of the two pair partners are determined by different mechanisms.

Since T_2 of ^{31}P in the interface-defect proximity is quenched drastically compared to bulk ^{31}P , and since this quenching is not due to the electronic transition, we conclude that the interface state induced T_2 process described by de Sousa¹⁵ is responsible for the observed ^{31}P T_2 times. The description of this mechanism predicts a relationship $T_2 \propto \frac{1}{\sqrt{n}}$ between the transverse spin relaxation time T_2 of near-interface ^{31}P donor electrons and the interface density n . For the given anneal parameters, the literature predicts a ratio $n_n/n_a \approx 4$ between the native interface density n_n and the annealed interface density n_a . Thus, the values of the T_2 times before and after annealing are expected to be $T_2^a/T_2^n \approx 2$. The experimentally observed value of $T_2^a/T_2^n = 2.1(9)$ as obtained from the high-field ^{31}P peak measurements in Table II is in full agreement with these predictions.

The confirmation of the de Sousa model allows a prediction of the distance of the interface from those ^{31}P atoms which contribute to the observed pEDMR signals. Assuming a native oxide interface state density of $n_n = 10^{13} \text{ cm}^{-3}$, we arrive at a ^{31}P to interface distance of $d \approx 4$ nm. Given the size of the s -shaped ^{31}P donor electron wave-function envelope we conclude that this is a reasonable value. We note however that this agreement occurs even though we are violating one of the assumptions of the de Sousa model—in these experiments, the average distance between interface defects is smaller than the distance of ^{31}P from the interface.

Our results have implications for quantum information concepts which aim to utilize ^{31}P donor spins close to the

c-Si/SiO₂ interface as qubits. The data presented above show that, without the ability to suppress the noise induced by interface defects, the extremely long coherence times of the ³¹P qubits seen in bulk ³¹P measurements are completely obliterated. This insight is particularly important for interface-defect based readout concepts. Even if ways are found to reduce the incoherence induced by these interface states, incoherence due to electronic transitions into the interface states will still need to be controlled, e.g., by control of the coupling between target and probe spins. This may be achieved by utilizing the Stark effect, as electric fields will have a stronger effect on the localization of the slightly delocalized ³¹P donor wave function in comparison to the extraordinary strongly localized deep interface defects. Whether these different electric field sensitivities have a significant impact on the exchange coupling between the ³¹P donors and interface states in close proximity and at sufficiently low fields remains to be seen. Finally, we note that the ability of spin-dependent transitions to reduce coherence times need to be considered for other potential ³¹P readout mechanisms discussed in the literature, such as spin-dependent scattering of conduction electrons by donor spins in two-dimensional electron gasses.^{48–53}

VI. SUMMARY

In summary, we have investigated spin-dependent processes at the *c*-Si:P/SiO₂ interface using pEDMR and shown that spin-dependent ³¹P to interface-defect recombi-

nation takes place at the *c*-Si(111) surface in a similar way to that seen with *c*-Si(100) surfaces. The imprints of spin-dependent recombination on interface currents reveal EPR resonances of the hyperfine split ³¹P resonance and P_b defects. At least one other defect is also seen, previously unobserved in ³¹P doped samples, and assigned here to the unrelaxed *E'* defect in the SiO₂ matrix. The correlation measurements of the dynamics of these pEDMR detected signals strongly support the model that recombination transitions between ³¹P and the interface-defect states occur.

By electrical detection of spin echoes, measurement of the coherence times *T*₂, as well as the longitudinal relaxation time *T*₁ of interface defects, and ³¹P donor spins in proximity to them, was possible. These measurements revealed that *T*₂ ≈ 1.3 μs for the P_b defect, independent of the applied temperature in the range 5 ≤ *T* ≤ 13 K. The *T*₂ time of ³¹P donor electrons is slightly longer and depends on the interface state density as described by de Sousa.¹⁵ The longitudinal relaxation time *T*₁ is consistently longer than the *T*₂ times and depends strongly on the P_b density. The measured *T*₁ for both P_b and ³¹P is the same, as expected for electrical readout using a spin-dependent electronic transition.

The observations contrast the pESR measured *T*₁ and *T*₂ of bulk ³¹P, which are significantly longer and strongly temperature dependent. The implications of these findings for possible applications of the ³¹P interface-defect transition as spin ³¹P readout for proposed potential spin electronics or quantum information applications have been discussed.

*dane.mccamey@physics.utah.edu

†boehme@physics.utah.edu

¹G. Feher and E. A. Gere, Phys. Rev. **103**, 501 (1956).

²G. Feher, Phys. Rev. Lett. **3**, 135 (1959).

³I. Appelbaum, B. Huang, and D. J. Monsma, Nature (London) **447**, 295 (2007).

⁴B. E. Kane, Nature (London) **393**, 133 (1998).

⁵R. G. Clark *et al.*, Philos. Trans. R. Soc. London, Ser. A **361**, 1451 (2003).

⁶H. Huebl, F. Hoehne, B. Grolik, A. R. Stegner, M. Stutzmann, and M. S. Brandt, Phys. Rev. Lett. **100**, 177602 (2008).

⁷A. M. Tyryshkin, S. A. Lyon, A. V. Astashkin, and A. M. Raitsimring, Phys. Rev. B **68**, 193207 (2003).

⁸J. J. L. Morton, A. M. Tyryshkin, R. M. Brown, S. Shankar, B. W. Lovett, A. Ardavan, T. Schenkel, E. E. Haller, J. W. Ager, and S. A. Lyon, Nature (London) **455**, 1085 (2008).

⁹C. Boehme and K. Lips, Phys. Status Solidi B **233**, 427 (2002).

¹⁰A. R. Stegner, C. Boehme, H. Huebl, M. Stutzmann, K. Lips, and M. S. Brandt, Nat. Phys. **2**, 835 (2006).

¹¹T. M. Buehler, V. Chan, A. J. Ferguson, A. S. Dzurak, F. E. Hudson, D. J. Reilly, A. R. Hamilton, R. G. Clark, D. N. Jamieson, C. Yang, C. I. Pakes, and S. Praver, Appl. Phys. Lett. **88**, 192101 (2006).

¹²V. C. Chan, T. M. Buehler, A. J. Ferguson, D. R. McCamey, D. J. Reilly, A. S. Dzurak, R. G. Clark, C. Yang, and D. N. Jamieson, J. Appl. Phys. **100**, 106104 (2006).

¹³T. Schenkel *et al.*, Microelectron. Eng. **83**, 1814 (2006).

¹⁴T. Schenkel, A. M. Tyryshkin, R. de Sousa, K. B. Whaley, J. Bokor, J. A. Liddle, A. Persaud, J. Shangkuan, I. Chakarov, and S. A. Lyon, Appl. Phys. Lett. **88**, 112101 (2006).

¹⁵R. de Sousa, Phys. Rev. B **76**, 245306 (2007).

¹⁶G. Lucovsky, Y. Wu, H. Niimi, V. Misra, and J. C. Phillips, Appl. Phys. Lett. **74**, 2005 (1999).

¹⁷K. Eng, R. N. McFarland, and B. E. Kane, Appl. Phys. Lett. **87**, 052106 (2005).

¹⁸K. Eng, R. N. McFarland, and B. E. Kane, Phys. Rev. Lett. **99**, 016801 (2007).

¹⁹Y. Nishi, Jpn. J. Appl. Phys. **10**, 52 (1971).

²⁰E. H. Poindexter, P. J. Caplan, B. E. Deal, and R. R. Razouk, J. Appl. Phys. **52**, 879 (1981).

²¹E. H. Poindexter, G. J. Gerardi, M.-E. Rueckel, P. J. Caplan, N. M. Johnson, and D. K. Biegelsen, J. Appl. Phys. **56**, 2844 (1984).

²²A. Stesmans, Z. Phys. Chem., Neue Folge **151**, 191 (1987).

²³Y. Y. Kim and P. M. Lenahan, J. Appl. Phys. **64**, 3551 (1988).

²⁴A. Stesmans and K. Vanheusden, Phys. Rev. B **44**, 11353 (1991).

²⁵P. M. Lenahan and J. F. Conley, J. Vac. Sci. Technol. B **16**, 2134 (1998).

²⁶R. Müller, P. Kanschat, S. von Aichberger, K. Lips, and W. Fuhs, J. Non-Cryst. Solids **266-269**, 1124 (2000).

²⁷D. R. McCamey, H. Huebl, M. S. Brandt, W. D. Hutchison, J. C.

- McCallum, R. G. Clark, and A. R. Hamilton, *Appl. Phys. Lett.* **89**, 182115 (2006).
- ²⁸D. R. McCamey, G. W. Morley, H. A. Seipel, L. C. Brunel, J. van Tol, and C. Boehme, *Phys. Rev. B* **78**, 045303 (2008).
- ²⁹F. Friedrich, C. Boehme, and K. Lips, *J. Appl. Phys.* **97**, 056101 (2005).
- ³⁰C. Boehme, F. Friedrich, T. Ehara, and K. Lips, *Thin Solid Films* **487**, 132 (2005).
- ³¹C. Boehme and K. Lips, *Physica B* **376-377**, 930 (2006).
- ³²K. L. Brower, *Appl. Phys. Lett.* **43**, 1111 (1983).
- ³³M. Cook and C. T. White, *Phys. Rev. B* **38**, 9674 (1988).
- ³⁴Y. Nishi, T. Tanaka, and A. Ohwada, *Jpn. J. Appl. Phys.* **11**, 85 (1972).
- ³⁵B. Koiller, X. Hu, and S. Das Sarma, *Phys. Rev. Lett.* **88**, 027903 (2001).
- ³⁶C. J. Wellard and L. C. L. Hollenberg, *Phys. Rev. B* **72**, 085202 (2005).
- ³⁷G. W. Morley, D. R. McCamey, H. A. Seipel, L. C. Brunel, J. van Tol, and C. Boehme, *Phys. Rev. Lett.* **101**, 207602 (2008).
- ³⁸G. Feher, *J. Phys. Chem. Solids* **8**, 486 (1959).
- ³⁹D. R. McCamey, H. A. Seipel, S.-Y. Paik, M. J. Walter, N. J. Borys, J. M. Lupton, and C. Boehme, *Nature Mater.* **7**, 723 (2008).
- ⁴⁰C. Boehme and K. Lips, *Phys. Rev. B* **68**, 245105 (2003).
- ⁴¹B. I. Shklovskii, H. Fritzsche, and S. D. Baranovskii, *Phys. Rev. Lett.* **62**, 2989 (1989).
- ⁴²A. Gliesche, C. Michel, V. Rajevac, K. Lips, S. D. Baranovskii, F. Gebhard, and C. Boehme, *Phys. Rev. B* **77**, 245206 (2008).
- ⁴³G. Feher and E. A. Gere, *Phys. Rev.* **114**, 1245 (1959).
- ⁴⁴D. Kaplan, I. Solomon, and N. F. Mott, *J. Phys. (Paris), Lett.* **39**, 51 (1978).
- ⁴⁵N. M. Atherton, *Principles of Electron Spin Resonance*, Physical Chemistry Series (Ellis Horwood and PTR Prentice Hall, Chichester, 1993).
- ⁴⁶A. Schweiger and G. Jeschke, *Principles of Pulse Electron Paramagnetic Resonance* (Oxford University Press, Oxford, 2001).
- ⁴⁷A. Stesmans, *Phys. Rev. B* **48**, 2418 (1993).
- ⁴⁸R. N. Ghosh and R. H. Silsbee, *Phys. Rev. B* **46**, 12508 (1992).
- ⁴⁹C. C. Lo, J. Bokor, T. Schenkel, A. M. Tyryshkin, and S. A. Lyon, *Appl. Phys. Lett.* **91**, 242106 (2007).
- ⁵⁰L. H. Willems van Beveren, H. Huebl, D. R. McCamey, T. Duty, A. J. Ferguson, R. G. Clark, and M. S. Brandt, *Appl. Phys. Lett.* **93**, 072102 (2008).
- ⁵¹H. Huebl, R. P. Starrett, D. R. McCamey, A. J. Ferguson, and L. H. Willems van Beveren, *Rev. Sci. Instrum.* **80**, 114705 (2009).
- ⁵²M. Sarovar, K. C. Young, T. Schenkel, and K. B. Whaley, *Phys. Rev. B* **78**, 245302 (2008).
- ⁵³R. de Sousa, C. Lo, and J. Bokor, *Phys. Rev. B* **80**, 045320 (2009).